Repeat-Associated MicroRNAs Trigger Fragile X Mental Retardation-Like Syndrome in Zebrafish

Shin-Ju E. Chang, Samantha Chang-Lin, Donald C. Chang, Chen Pu Chang, Shi-Lung Lin* and Shao-Yao Ying*

Department of Cell & Neurobiology, Keck School of Medicine, University of Southern California, CA, USA

Abstract: A new class of repeat-associated microRNA (ramRNA) is identified to hinder normal brain development in zebrafish. Previous studies have shown that small hairpin RNAs derived from the 5'-untranslational CGG/CCG trinucleotide repeat [r(CGG)] expansion of fragile X mental retardation gene 1, *FMR1*, may cause neuronal toxicity in fragile X mental retardation syndrome (FXS). However, their roles in FXS remain unclear. We report here that over-expression of a novel ramRNA species isolated from the fish *FMR1* r(CGG) region triggers FXS-like neurodegeneration in a transgenic zebrafish model. Hyper-methylation of the *FMR1* 5'-r(CGG) region associated with ramRNA over-expression is central to this FXS-like etiology. Such an epigenetic modification results in the transcriptional inactivation of the *FMR1* gene and deficiency of its protein FMRP. FMRP deficiency further causes neurite deformity and synaptic dysfunction in the hippocampal neurons essential for cognition and memory. These findings provide significant insights into the role of ramRNAs in the embryonic brain development.

Keywords: MicroRNA (miRNA), CGG trinucleotide repeat, FMR1, transcriptional gene silencing, brain development, fragile X syndrome (FXS), mental retardation.

INTRODUCTION

A large portion of the genome is non-coding DNA, which often contains microsatellite-like short nucleotide repeats with unknown function. Recent studies have shown that certain trinucleotide repeats can fold into RNA hairpins, which in turn are further processed by RNaseIII-associated *Dicer* to form microRNA (miRNA)-like molecules [1, 2]. These ramRNAs may play crucial roles in several triplet repeat expansion diseases (TREDs), including fragile X syndrome (FXS), Huntington's disease (HD), myotonic dystrophy (DM), and a number of spinocerebellar ataxias (SCAs). But, the pathogenic mechanism underlying these diseases is unclear. For FXS, two theories have been proposed. First, small non-coding RNAs transcribed from the r(CGG) expansion of the *FMR1* 5'-untranslated region (5'-UTR) can fold into RNA hairpins, which may serve as a possible substrate for the *Dicer* processing [1]. Second, the RNA hairpins may reversely interact with the 5'-UTR r(CGG) region and inactivate the *FMR1* gene transcription [3]. Conceivably, the *FMR1* r(CGG)-derived ramRNA is likely involved in the formation of RNA-induced transcriptional silencing (RITS) assembly near the *FMR1* promoter, resulting in epigenetic repression of the *FMR1* chromatin locus.

FXS is the most common form of inherited mental retardation, taking up 30% of total human mental retardation disorders. It is also one of the most frequent single gene disorders [4]. This mental disorder is originated from the deficiency of an *FMR1*-encoded protein, FMRP. FMRP is associated with polyribosome assembly in a ribonucleoprotein (RNP)-dependent manner and suppresses certain protein translation involved in neuronal development and plasticity [3]. FMRP also contains a nuclear localization signal (NLS) and a nuclear export signal (NES) for shuttling certain mRNAs between the nucleus and cytoplasm [5, 6]. Given that the *FMR1* gene is inactivated by the trinucleotide expansion (i.e. ≥200 CGG copies) and the methylation of r(CGG) in 99% of FXS patients during embryonic development [7], the mechanism underlying such a transcriptional *FMR1* inactivation may shed light on the causes of FXS. We propose that the expansion of *FMR1* r(CGG) elevates the r(CGG)-derived ramRNA concentration, which in turns increases the *FMR1* gene methylation and inactivation in certain brain neurons vital to cognition and memory.

To test the effect of *FMR1* r(CGG)-derived ramRNA over-expression on brain development, we first identified and isolated a native fish *fmr1* 5'-untranslational r(CGG) region from an *actin* promoter-driven EGFP-expressing Tg(*actin*-GAL4:UAS-gfp) strain zebrafish (Fig. **1**, the sequence between two black arrows). We have also determined the sequence and methylation map of a 450-nucleotide area surrounding the isolated r(CGG) region [8]. Then, the RNA transcript of this r(CGG) region was transgenically over-expressed in the Tg(*actin*-GAL4:UAS-gfp) zebrafish by retroviral delivery. Zebrafish (*Danio rerio*) have served as an excellent model for studying human mental disorders, including FXS and autism [9]. They possess three *FMR1*-related familial genes, *fmr1*, *fxr1* and *fxr2*, which are orthologous to the human *FMR1*, *FXR1* and *FXR2* genes, respectively [10]. The tissue expression patterns of these familial genes in zebrafish are broadly consistent with those

*Address correspondence to these authors at the Department of Cell & Neurobiology, Keck School of Medicine, University of Southern California, 1333 San Pablo Street, BMT-403, Los Angeles, California 90033, USA; Tel: 0021-323-442-1856; Fax: 0021-323-442-3466; E-mail: syingusc.edu or linsusc.edu

1876-5238/08

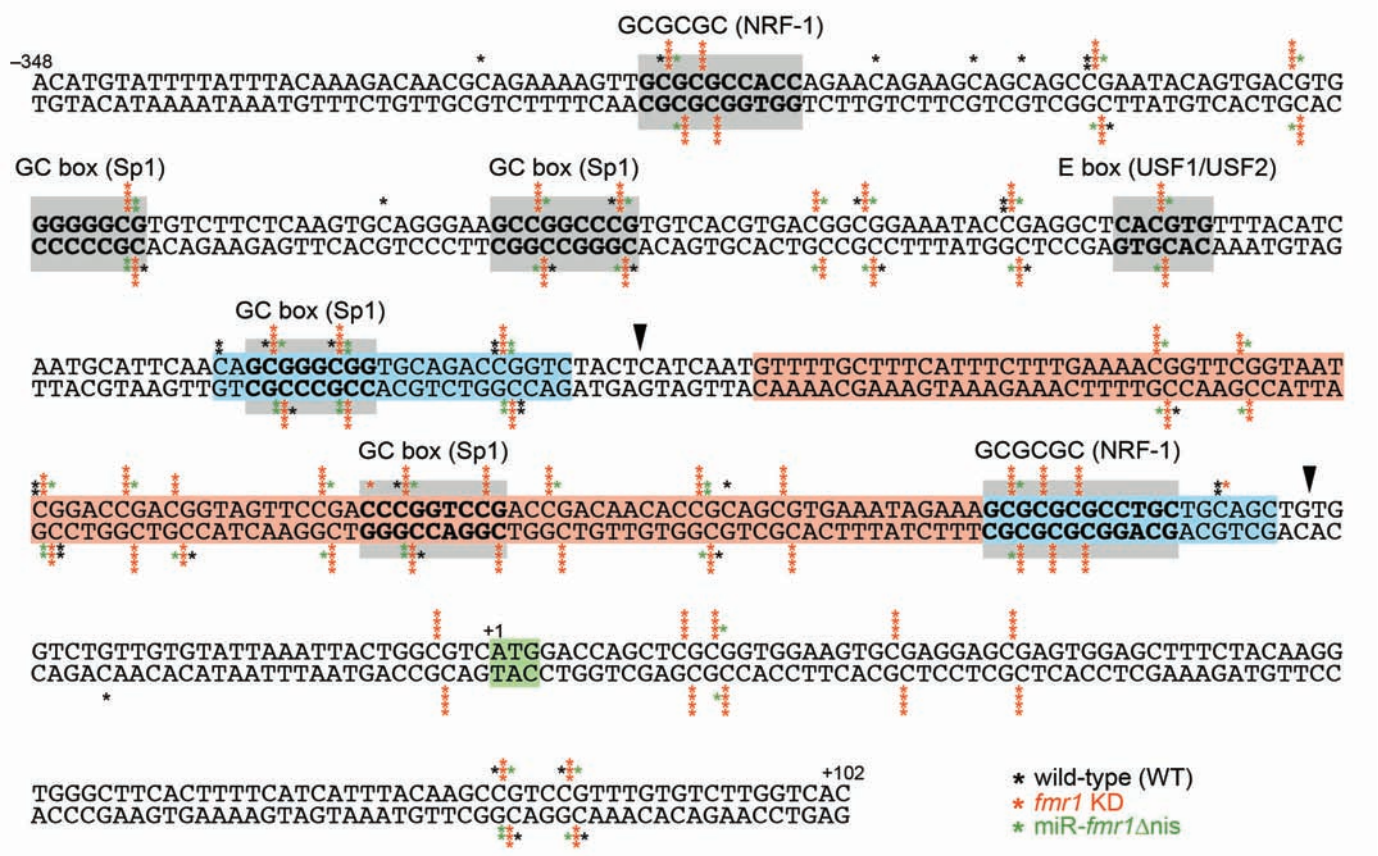

Fig. (1). Sequence and DNA methylation maps of the *fmr1* 5'-untranslational r(CGG) region found in WT (black), *fmr1* KD (red), and miR-*fmr1*Δnis (green) pallium neurons of the Tg(*actin*-GAL4:UAS-gfp) strain zebrafish (n = 5), determined by bisulfite PCR and DNA sequencing. Each asterisk (*) mark indicated a positively methylated site in the DNA sequence. The boxes in gray, blue, red, and green represented the transcription factor binding sites, focal methylation sites, miR-*fmr1*-targeted sites, and translation start codon, respectively.

of humans [10, 11]. As shown in Fig. (**2**), we modified a VSV-G positive pantropic retroviral vector, namely *pGABAR2-rT-SpRNAi*, to deliver a recombinant *SpRNAi-rGFP* transgene, which expresses a precursor miRNA (pre-miRNA)-containing intron transcript, such as the isolated *fmr1* r(CGG) RNA. The vector-dependent gene transcription is modulated by an isolated gamma-aminobutyric acid receptor *ßZ2* (*GABAR2*). This type of intronic miRNA-mediated transgenic approach has been successfully used to ectopically express mature miRNAs and silence their targeted genes in several animal systems, including zebrafish, chicken and mouse [12-14]. Given that *GABAR2* and *FMR1* genes were co-expressed in the GABAergic neurons of cortex, hippocampus and cerebellum [15, 16], the isolated *fmr1* r(CGG) RNA was thus transcribed specifically in the *FMR1*-positive neurons and consequently prevented any potential off-target effect in other neurons.

Given that increasing viral concentrations during infection leads to high multiplicity of infection (MOI), we can control the levels of MOI and r(CGG)-derived RNA expression in zebrafish through manipulating the retroviral concentrations during transgene delivery. As illustrated in Fig. (**3A**), the wild-type Tg(*actin*-GAL4:UAS-gfp) strain zebrafish contain less than 50 copies of r(CGG), whereas the r(CGG) number in FXS is assumed to be larger than 200, which conceivably generates over four times of r(CGG)-derived RNAs directed against the *fmr1* 5'-untranslational r(CGG) region. Given that the r(CGG) in our transgenic zebrafish is the same as that of the wild-type Tg(*actin*-GAL4:UAS-gfp) fish, we forced the elevation of *fmr1* r(CGG)-derived RNA expression by retroviral delivery of the r(CGG) RNA-expressing *SpRNAi-rGFP* transgene into the zebrafish genome. By this means, we successfully measured the effect of concentrated r(CGG)-derived RNA accumulation and observed a FXS-like disorder in the targeted GABAergic neurons with an elevated r(CGG)-derived RNA level over six folds.

MATERIALS AND METHODOLOGY

Construction of the SpRNAi-rGFP Transgene Containing the Fish fmr1 5'-UTR r(CGG) Insert

The *SpRNAi-rGFP* transgene consisted three parts: one artificial intron, namely *SpRNAi*, and two exons derived from a mutated red fluorescent HcRed1 chromoprotein gene isolated from *Heteractis crispa*, namely *rGFP* [17, 18]. Synthetic oligonucleotides used for generating the *SpRNAi* intron were: sense phosphorylated 5'-GTAAGTGGTC CGAT CGTCGC GACGCGTCAT TACTAACTAT CAATATCT TA ATCCTGTCCC TTTTTTTTCC ACAGTAGGAC CTT CGTGCA-3' and antisense 5'-TGCACGAAGG TCCTAC TGTG GAAAAAAAAG GGACAGGATT AAGATATTGA TAGTTAGTAA TGACGCGTCG CGACGATCGG ACCA CTTAC-3' (Sigma-Genosys, Woodlands, TX). The *SpRNAi*

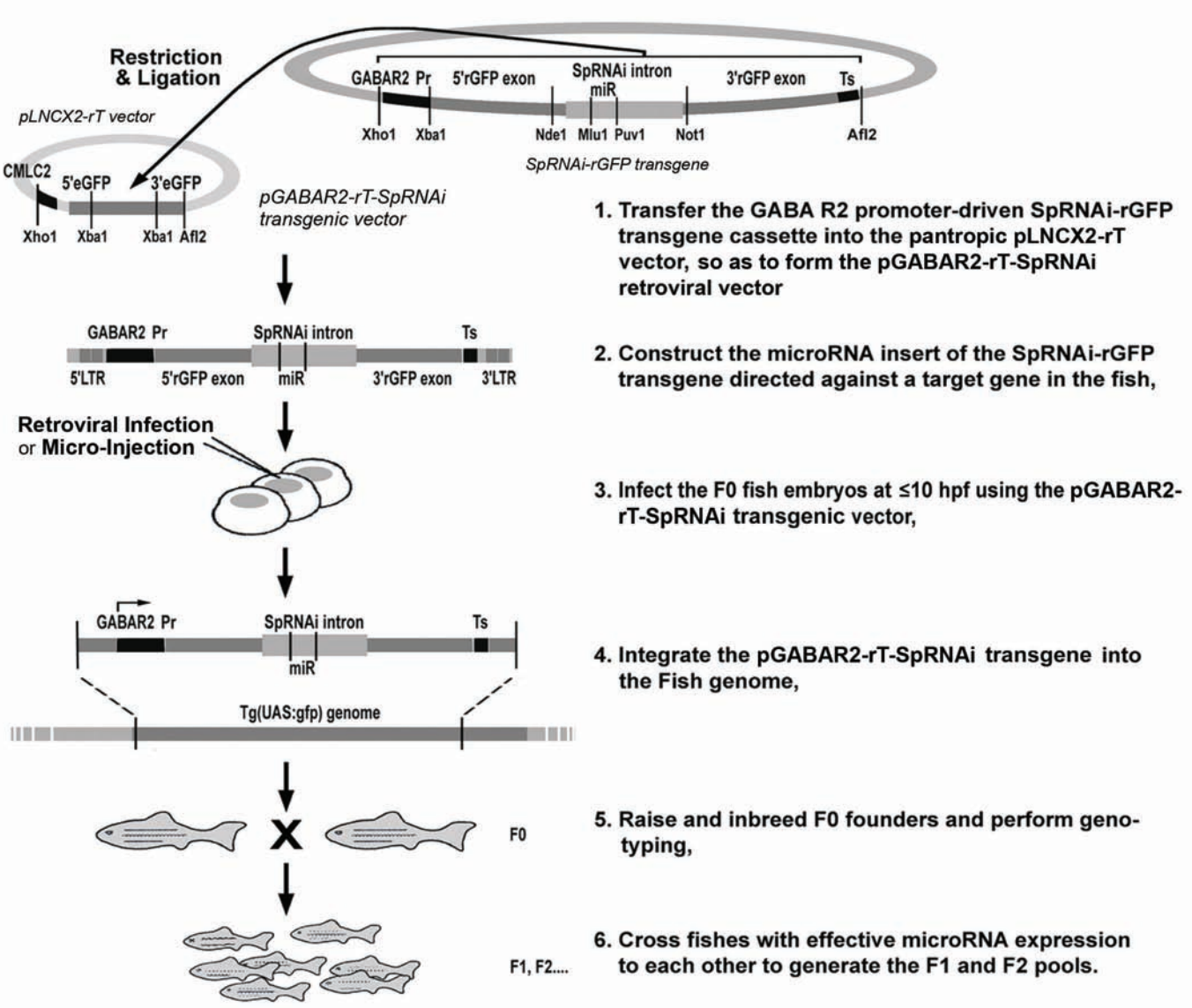

Fig. (2). Schematic protocol for retroviral delivery of a ramRNA-expressing transgene into zebrafish. A transgenic *pGABAR2-rT-SpRNAi* retroviral vector was developed and used to insert a pre-designed *SpRNAi-rGFP* transgene into the genome of Tg(*actin*-GAL4:UAS-gfp) zebrafish for steady transgene expression (supplemental references *1-3*). An r(CGG)-derived ramRNA precursor isolated from the fish *fmr1* 5'-UTR r(CGG) expansion (homologous to accession number NW001511047 from the 124001st to 124121st nucleotide) was inserted in the *SpRNAi* intron region of the *SpRNAi-rGFP* transgene and then co-expressed with the transgene in zebrafish. The transgene expression was driven by a neuron-specific fish *GABA(A) receptor βZ2* (*GABAR2*) promoter. The *fmr1* KD zebrafish line was established following the procedures listed in the right panel.

intron was formed by the hybridization of equal ratio (1:1) for each sequence at 94℃ for 2 min, 70℃ for 10 min and then 4℃ in 1 x PCR buffer (50 mM Tris-HCl, pH 9.2 at 25℃, 16 mM $(NH_4)_2SO_4$, 1.75 mM $MgCl_2$). Next, the hybridized *SpRNAi* intron was purified with a microcon-30 filter (Amicon, Beverly, MA) in 10 μl of autoclaved ddH_2O, and then cleaved by a *DraII* restriction enzyme (10 U) at 37℃ for 4 hours. The cleaved intron was collected with a new microcon-30 filter in 10 μl of autoclaved ddH_2O. Concurrently, two *rGFP* exon sequences were generated by *DraII* through enzymatic cleavage in the 208th nucleotide (nt) site of the HcRed1 gene (BD Biosciences, Palo Alto, CA). The 5'-end exon fragment was further blunt-ended by T4 DNA polymerase (5 U).

The *SpRNAi-rGFP* transgene was formed by ligation of the *SpRNAi* intron and the two *rGFP* exons. We first mixed equal ratios (1:1:1) of the intron and exons, and incubated the mixture in 1 x PCR buffer from 50℃ to 10℃ over a period of 1 hour. Then, T_4 DNA ligase (20 U) and buffer (Roche Biochemicals, Indianapolis, IN) were added into the mixture and ligation was carried out in 12℃ for 12 hours. To clone the entire *SpRNAi-rGFP* transgene, the ligated products (10 ng) were amplified by high-fidelity PCR (Roche) with a pair of primers (sense 5'-CTCGAGCATG GTGAGCGGCC TGCTGAA-3' and antisense 5'-dTCTAGAAGTT GGCCTTCTCG GGCAGGT-3') at 94℃ for 1 min, 54° for 1 min and then 68℃ for 2 min for 25 cycles. The PCR products were fractionated on a 2% agarose gel, and a ~900 base-pair (bp) sequence was extracted and

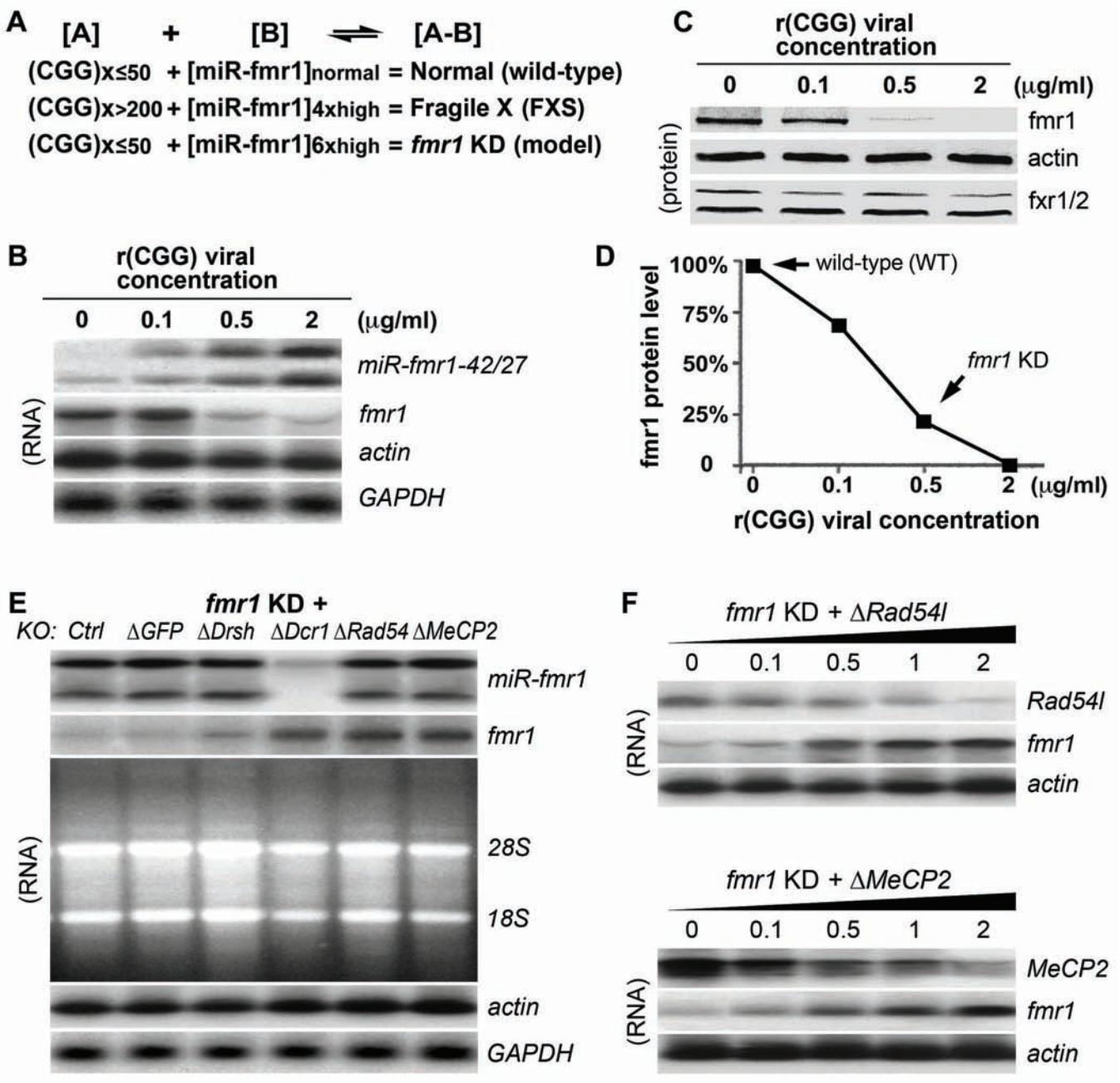

Fig. (3). Model of the transgenic *fmr1* KD zebrafish mimicking human FXS. (**A**) Normal *fmr1* 5'-UTR contains 35-50 CGG repeats [r(CGG)], whereas the estimated r(CGG) number in FXS is over 200. After over-expression of the normal *fmr1* r(CGG) up to 6 folds, the *fmr1* KD zebrafish displayed a phenotype similar to FXS. (**B**) Dose-dependent correlation between r(CGG)-derived miR-*fmr1* expression and knockdown of the target *fmr1* mRNA, determined by northern blotting (n = 5, $p < 0.01$). The increase of miR-*fmr1* expression was directly proportional to the transfection rates of the *pGABAR2-rT-SpRNAi* vector. (**C**) Dose-dependent knockdown of the target fmrp protein as determined by western blot analysis (n = 5, $p < 0.01$). (**D**) Line chart display of the result (C). Arrows indicate the two comparisons: the wild-type (WT) and the transgenic zebrafish with 75%-85% *fmr1* and fmrp knockdown (*fmr1* KD). (**E**) Involvement of RNAi- and DNA methylation-associated genes in the *fmr1* KD zebrafish (n = 7, $p < 0.01$). Morpholino antisense oligonucleotide-mediated gene knockdown was directed against green fluorescent protein (Δ*GFP*), fish *Drosha* (Δ*Drsh*), *Dicer1* (Δ*Dcr1*), *Rad54-like* (Δ*Rad54*), and *MeCP2* (Δ*MeCP2*), in that order. (**F**) Dose-dependent correlation between the knockdown of *Rad54l* and *MeCP2* and the restored expression of *fmr1* mRNA in the *fmr1* KD zebrafish (n = 4, $p < 0.01$).

purified by a gel extraction kit (Qiagen, Valencia, CA). The nucleotide composition of the *SpRNAi-rGFP* transgene was further confirmed by DNA sequencing.

Insertion of the SpRNAi-rGFP Transgene into the pGABAR2-rT-SpRNAi Retroviral Vector

We modified a *VSV-G*-positive pantropic retroviral vector, namely *pLNCX2-rT* (Clontech Palo Alto, CA), to trans-

genically deliver the *fmr1* 5'-UTR r(CGG)-encoded *SpRNAi-rGFP* transgene [13]. The *pLNCX2-rT* vector was derived from a modified pseudotype Moloney Murine Leukemia virus, *pLNCX2* (Clontech) [13]. As shown in Fig. (**2**), we first incorporated the *SpRNAi-rGFP* transgene into the *XhoI/AflII* restriction site of the *pLNCX2-rT* vector to form a retroviral *pGABAR2-rT-SpRNAi* transgene vector capable of transgenically expressing the isolated *fmr1* r(CGG) in zebrafish. Experimentally, we mixed equal ratios (1:1) of the *SpRNAi-rGFP* transgene and the *pLNCX2-rT* retroviral vector. Then, the mixture was cleaved with *XhoI* and *AflII* restriction enzymes at 37℃ for 4 hours. Afterwards, the cleaved mixture was collected with a microcon-30 filter and ligation was performed with T_4 DNA ligase (20 U, Roche) at 12℃ for 12 hours. The *fmr1* r(CGG)-inserted *pGABAR2-rT-SpRNAi* vector was propagated in *E. coli* DH5α LB cultures containing 100 μg/ml ampicillin (Sigma) and purified with a QIAprep spin miniprep kit (Qiagen). For viral production, the *pGABAR2-rT-SpRNAi* vector was co-transfected with an equal amount of *pVSV-G* vector into GP2-293 packaging cells (Clontech) to produce infectious, non-replicable, pantropic retroviruses. GP2-293 cells were grown in phenol red-free DMEM medium supplemented with 10% FBS, 4 mM L-glutamine and 1 mM sodium pyruvate. High titer viruses were collected from the DMEM medium of the GP2-293 cell cultures approximately 36-48 hours after the co-transfection. The viral titer was measured using a retro-X qRT-PCR titration kit (Clontech).

Generation of Transgenic fmr1 KD Zebrafish Lines Using the pGABAR2-rT-SpRNAi Retroviral Vector

Our transgenic zebrafish lines were grown and maintained following the protocols of the Zebrafish Book [19]. The developmental stages of zebrafish were determined according to criteria described by Kimmel *et al.* [20]. For preparing high-titer viruses, 15 ml of 1x DMEM medium from the co-transfected GP2-293 packaging cell culture was collected and filtrated through a 0.45 μm filter and viral particles were pelleted by 25,000 x *g* ultracentrifuge for 2 hours at 4˚C and re-suspended in ice-cold 1x phosphate buffered saline (PBS). The viral titer was measured according to the protocol of a retro-X qRT-PCR titration kit (Clontech). For transgenic fish generation, zebrafish fertilized eggs were dechorinated by pronase digestion [19] and 1.0 nl of the concentrated viral solution was microinjected into the dechorinated one-cell fish embryos, using a pair set of MO-188NE 3D hydraulic fine micromanipulators and a microinjector under a TE2000 invert microscopic system (Nikon). At 3-month post-fertilization, we isolated genomes from the caudal fin clips of the F0 transgenic zebrafish by incubating in a solution consisting of 10 mM Tris-HCl (pH 8.0), 10 mM EDTA, and 0.2 mg/ml proteinase K for 3 hours at 55℃. Genotyping was performed with PCR to detect the *SpRNAi-rGFP* transgene, using a pair of primers 5'-TCCAGGAGCG CACCATCTTC-3' and 5'-AACTCCAGCA GGAC-CATGTG-3' at 94℃ for 1 min and then 68℃ for 2 min for 30 cycles. Afterwards, northern blot and western blot analyses were used to measured the expression of r(CGG)-derived miR-*fmr1* and its targeted *fmr1* mRNA and fmrp protein, respectively. After that, the F0 transgenic zebrafish were selectively separated into four groups showing losses of <50%, 50%-75%, 75%-90%, and >90% of *fmr1* and fmrp expression, as determined by both northern and western blot analyses. While the zebrafish manifesting >90% *fmr1* knockdown failed to form a transgenic line, we have succeeded in mating the fish with a 75%-90% *fmr1* knockdown rate to form the F1 founder line with a stable 75%-85% *fmr1* knockdown rate.

Morpholino Antisense Oligonucleotide-Mediated Gene Knockdown

Synthetic morpholino oligonucleotide probes (Gene Tools, Philomath, OR) were composed of anti-*zfDrosha* (Δ*Drsh* 5'-CACACGTCCT CGGTCATAGT C-3'), anti-*zfDicer1* (Δ*Dcr1* 5'-CCTCTTCATC ATGCAGGTCC A-3'), anti-*Rad54l* (Δ*Rad54* 5'-CCTCACACCA GCTCGTCTCA-3'), and anti-*MeCP2* (Δ*MeCP2* 5'-GAGAGCAGCT CCAACTTCAG G-3'). Fertilized one-cell zebrafish embryos were dechorinated by pronase digestion and then microinjected with 1.0-nl volume 2.0 ng of the morpholino oligonucleotides. Each treatment group contained at least thirty fish embryos. After 12-hour incubation, we confirmed the knockdown of the morpholino-targeted mRNA in each treatment group by northern blot analysis as described below.

Northern Blot Analysis

At 72-hour post-fertilization (hpf), we homogenized ten F2 zebrafish larvae originated from the same F1 transgenic group in liquid nitrogen and isolated total RNAs using RNeasy spin columns (Qiagen, Valencia, CA). The total RNAs (10 μg) were fractionated on 1% formaldehyde-agarose gels and transferred onto nylon membranes (Schleicher & Schuell, NH). Synthetic probes (Sigma-Genosys, Woodlands, TX) were prepared, including anti-miR-*fmr1* [LNA]-DNA (5'-[CGGTGTTGTC] GGTCGGAC CG GGTCGGA-3') and antisense DNA targeting against the sequences of *fmr1* nucleotide (nt) 1803-1931 (accession number NM152963), the zebrafish *Drosha-like RNaseIII* nt 831-951 (accession number XM690799), the *Dicer1* nt 241-361 (accession number AY386319), the *Rad54-like* nt 540-661 (accession number NM201144), and the *MeCP2* nt 181-300 (accession number NM212736). All probes were purified by PAGE gel extraction. Each probe was tail-labeled with terminal transferase (20 U) for 20 min in the presence of [^{32}P]-dATP (> 3000 Ci/mM, Amersham International, Arlington Heights, IL) and then hybridized to the membrane blot. The probes contained no complementarity to each other or other known genes in particular, *fxr1* and *fxr2*. Hybridization was carried out in a mixture of 50% freshly deionized formamide (pH 7.0), 5 x Denhardt's solution, 0.5% SDS, 4 x SSPE, and 250 μg/μL denatured salmon sperm DNAs (42℃ for 18 hours). Membranes were sequentially washed twice in 2 x SSC, 0.1% SDS (25℃ for 10 min), and once in 0.1 x SSC and then 0.1% SDS (42℃ for 30 min) before autoradiography.

Western Blot Analysis

At 72-hpf, we homogenized ten F2 zebrafish larvae originated from the same F1 transgenic group and lysed with a CelLytic-M lysis/extraction reagent (Sigma-Aldrich, St. Louis, MO) supplemented with protease inhibitors, Leupeptin, TLCK, TAME and PMSF. The total protein volume

was determined using an improved SOFTmax protein assay package on an E-max microplate reader (Molecular Devices, CA). Each 30 μg of cell lysate was added to SDS-PAGE sample buffer under reducing (+50 mM DTT) and non-reducing (no DTT) conditions and boiled for 3 min before loading onto 4~8% polyacylamide gels; molecular weights were determined by comparison to standard proteins (Bio-Rad, Hercules, CA). Proteins were resolved by SDS-polyacrylamide gel electrophoresis (PAGE) and then electroblotted onto a nitrocellulose membrane and incubated in Odyssey blocking reagent (Li-Cor Biosciences, Lincoln, NB) for 2 hours at room temperature. Then, a primary antibody was applied and mixed to the membrane blot and incubated at 4℃ overnight. The primary antibodies included FMR1 (1:500, Chemicon, Temecula, CA), actin (1:2000, Chemicon), and rGFP (1:1000, Clontech, Palo Alto, CA). The FMR1 antibody cross-reacted to fmr1, fxr1 and fxr2, which could be distinguished based on their various sizes in the western blots. After incubation, the membrane was rinsed three times with TBS-T and then exposed to a goat anti-mouse IgG secondary antibody conjugated with an Alexa Fluor 680 reactive dye (1:2,000; Invitrogen-Molecular Probes) for 1 hour at room temperature. After three additional TBS-T rinses, we conducted a fluorescent scan of the immunoblot and image analysis using Li-Cor Odyssey Infrared Imager and Odyssey Software v.10 (Li-Cor).

Fluorescent *In Situ* Hybridization (FISH) Assay

Zebrafish were euthanized in a 0.2 gl^{-1} solution of tricaine (3-amino-benzoic ethylester) and embedded in Tissue-Tek (Sigma-Aldrich). Then the samples were fixed at room temperature for 10 min in 4% paraformaldehyde in 0.1 mol^{-1} Sorrensen buffer (pH 7.3), followed by a permeabilization step in 100% methanol for 20 min. The samples were washed sequentially with 1x PBS, methanol, isopropanol and tetrahydronaphthalene before being embedded in paraffin wax. The embedded samples were cut on a microtome at 7 μm thickness and mounted on clean TESPA-coated slides. The FISH assay kit was purchased from Ambion Inc. (Austin, TX) and performed according to the manufacturer's suggestion. We used a synthetic Alexa Fluro 647-labeled [LNA]-DNA probe (Sigma-Genosys) targeting against miR-*fmr1-27* (5'-[CGGTGTTGTC] GGTCGGACCG GGTCGGA-3'). The section slides were dewaxed with xylene, pre-fixed in 4% paraformaldehyde for 30 min, then digested with proteinase K (10 μg/ml; Roche Biochemicals, Indianapolis, IN) for 10 min at 37℃, re-fixed with 4% paraformaldehyde, and washed in Tris/glycine buffer. Nuclear membranes were further treated with a detergent buffer (10 mM Tris-HCl, pH 7.4, 100 mM NaCl, 5 mM $MgCl_2$, 1 mM EDTA, 4 mM vanadyl adenosine, 1.2 mM phenylmethylsulfonyl fluoride, 1% (v/v) Tween 40, and 0.5% (v/v) sodium deoxycholate) for 5 min at 4℃ and washed three times in Tris/glycine buffer. After that, the slides were hybridized overnight at 60℃ within the cloverslip chambers in *in situ* hybridization buffer (40% formamide, 5x SSC, 1x Denhard's solution. 100 μg/ml salmon testis DNA, and 100 μg/ml tRNA), containing 1 ng/μl of the labeled LNA-DNA probe. After post-hybridization, we washed the slides once with 5x SSC and once with 0.5x SSC at 25℃ for 1 hour. Positive results were observed under a 100x microscope with whole field z-axis stacking (up to 40 μm) scanning and recorded at 200x, 400x and 1,000x magnification (Nikon 80i and TE2000 microscopic quantitation systems).

Bisulfite PCR and Genomic DNA Sequencing

Genomic DNAs from the palliums of three-month-old zebrafish were isolated with a DNA isolation kit (Roche). The DNAs (2 μg) were used for PCR cloning of the 450-bp 5'-regulatory region of the *fmr1* promoter, before and after bisulfite modification. Bisulfite modification was performed with a CpGenome DNA medification kit (Chemicon). The bisulfite treatment converted all unmethylated cytosines to uracils while methylated cytosines remained as cytosines. Thus, methylation-specific PCR was carried out in triplicate to detect the presence of methylated and unmethylated (CGG/CCG) repeats in the isolated *fmr1* promoter region. We used a pair of synthetic primers 5'-TTTGATTTTG TTTGAGTATA ATATTC-3' and 5'-TCAAAACAAA CCATCAACAC CAAAC-3 for unmethylated DNA amplification, and another pair of primers 5'-TTCGATTTCG TTCGAGTATA ATA-3' and 5'-TCGAAACGAA CCATCGACAC CA-3' for methylated DNA amplification. After 35 cycles of PCR at 95℃ for 30 sec and 60℃ for 1 min, the amplified DNA products were separately purified by 2% agarose gel electrophoresis and extraction (Qiagen) and then used for DNA sequencing to identify the methylation sites. A DNA methylation map was generated by comparing the unchanged cytosines in the bisulfite-modified DNAs to those in the non-modified DNAs.

Reagent Preparation

(*S*)-3,5-dihydroxyphenyglycine (DHPG; 100 μM), D-2-amino-5-phosphonovalerate (D-APV; 50μM), picotoxin (20 μM), anisomycin (20 μM), and LY341495 (100 μM) were purchased from Sigma-Aldrich and prepared fresh in artificial cerebrospinal fluid (ACSF), consisting of 124 mM NaCl, 5mM KCl, 1.25 mM NaH_2PO_4, 26 mM $NaHCO_3$, 1 mM $MgCl_2$, 2 mM $CaCl_2$, and 10 mM dextrose (pH 7.4), and saturated with 95% O_2, 5% CO_2.

Analysis of Field Potentiation (FP) Analysis ($p < 0.01$, $n = 6$)

Three-month-old male zebrafish were first euthanized in a 0.2 gl^{-1} solution of tricaine (3-amino-benzoic ethylester) and their brain slices (40 μm) were cut on a vibratome and collected in ice-cold dissection buffer containing 212 mM NaCl, 2.6 mM KCl, 1.25 mM NaH_2PO_4, 26 mM $NaHCO_3$, 5 mM $MgCl_2$, 0.5 mM $CaCl_2$, and 10 mM dextrose. Immediately after, the slices were recovered for 3 hours at 30℃ in the ACSF solution saturated with 95% O_2, 5% CO_2. Field potentials were recorded with extracellular recording electrodes (1.0 MΩ) filled with ACSF in the target neuron region. We evoked synaptic responses through a 200-μsec current pulse with a concentric bipolar tungsten stimulating electrode (bipolar, insulated stainless 50 μm diameter wires). Stable base-line responses were collected every 30 sec using the stimulus intensity (10-30 μA) to yield 50%-60% of the maximal response. When a population spike appeared, the response to the highest-intensity stimulus not evoking a population spike was taken as the maximal field EPSP (fEPSP), and this value was used for the response to all higher intensities. The time-matched normalized data were

averaged across experiments and expressed in the text and figures as the means (± SEM). Significant differences between groups were determined using the independent *t* test and Komolgarov-Smirnov test.

Analysis of Long-Term Potentiation (LTP) ($p < 0.01$, $n = 4$)

We first measured the peak amplitude of dendritic fEPSP. Two responses were collected at each intensity and averaged. Baseline stimulus intensity was set to evoke 50%-60% of fEPSP. Paired-pulse curves were determined by stimulating the synapses with twin pulses at interpulse intervals of 50-1600 ms. The initial slope and peak amplitude of the response to the second (test) pulse were calculated as a percentage of those of the first (conditioning) pulse of each pair. Two sets of LTP were measured: one was induced after perfusing the slices with picrotoxin (20 μM) to block $GABA_A$-dependent synaptic inhibition, while the other was induced directly from non-treated slices. Theta burst stimulation (TBS; 5 Hz) was used to induce LTP. Different TBS intensities were given from counter direction; for example, five TBS from one pole while ten TBS from the other pole were given simultaneously. Two induction events were separated by at least 30 min. During TBS, the stimulation duration was doubled to 0.2 ms. The fEPSPs were monitored from both directions, alternatively, at 10 s intervals for 10 min before TBS and 60 min after. The degree of potentiation induced by TBS was calculated as the percentage increase at each point of time after patterned stimulation in relation to the baseline average.

Analysis of Long-Term Depression (LTD) ($p < 0.01$, $n = 4$)

LTD consists two forms, the *N*-methyl-D-aspartate receptor (NMDAR)-mediated LTD (NMDAR-LTD) and the group 1 metabotropic glutamate receptor (mGluR1)-dependent LTD (mGluR-LTD). We first induced LTD in the presence of a NMDAR antagonist, D-APV (50 μM), using paired-pulse low-frequency stimulation consisting of 900 pairs of stimuli (50-msec interstimulus interval) delivered at 1 Hz for 20 min. Extracellular field potentials (FPs) were measured in the stratum radiatum of lateral pallium elicited by the stimulation. The mGluR-dependent LTD (mGluR-LTD) was stimulated by application of 100 μM 3,4-dihydroxyphenylglycine (DHPG) for 2 min. Synaptic strength was measured as the initial slope (10%-40% of the rising phase of the FP). The LTD magnitude was compared at 60-70 min after the onset of DHPG between inhibitor-treated and control interleaved slices. Statistical significance was determined by independent *t*-tests.

Statistical Considerations

All numerical data were summarized *via* descriptive statistics: Mean, standard deviation (SD), minimum, maximum, *etc*. For comparison between two treatment groups, pairwise two-sample *t* test, nonparametric tests, chi-square analysis and Fisher's exact test were used. For experiments involving more than two treatment groups, analysis of variance test was performed followed by a multiple range test. A *p* value of less than 0.05 was considered as statistically significant. We used SPLUS and SAS statistical software for analysis.

RESULTS

Models of ramRNA-Induced fmr1 Gene Silencing in Zebrafish and the Identity of ramRNAs

The F0 transgenic zebrafish resulting from the retroviral *pGABAR2-rT-SpRNAi* infection were separated into four groups according to their distinct knockdown rates of *fmr1* mRNA and the *fmr1* protein fmrp, as determined by northern and western blotting. As shown in Fig. (**3B-D**), groups 1-4 showed a gradient decrease from 75%-100% (wild-type), 25%-75% (0.1 μg/ml retroviral insertion), 10%-25% (0.5 μg/ml), to <10% (2 μg/ml) of both *fmr1* mRNA and fmrp expression, respectively. This *fmr1* gene silencing effect was highly target-specific because other *FMR1*-related familial members, such as fxr1 and fxr2, and the house-keeping gene ß-actin were not affected by the transfection (Fig. **3C**). The zebrafish with less than 10% of *fmr1*/fmrp expression were incapable of mating; however, we were able to raise the fish with 10%-25% of *fmr1*/fmrp expression to form a F1 founder line with a consistent 75%-85% *fmr1*/fmrp knockdown rate, namely *fmr1* KD strain. The genotypes of the F1 and F2 *fmr1* KD lines were further confirmed by PCR and sequencing of the genomic transgene DNA, which showed two concomitant copies of the transgene inserted in the chromosome 18 close to the 3'-proximity of the LOC565390 locus region, where no known gene was encoded.

In these *fmr1* KD zebrafish, we have identified and isolated an r(CGG)-derived ramRNA, namely miR-*fmr1*, which were involved in the transcriptional inactivation of *fmr1* expression through DNA methylation. As shown in Fig. (**3B**) northern blotting, two primary miR-*fmr1* isoforms, miR-*fmr1-27* and miR-*fmr1-42*, were derived from the *fmr1* 5'-untranslational r(CGG) expansion region approximately 65-nucleotide upstream of the translational start codon (accession number NM152963). The transcription of *fmr1* mRNA was gradually attenuated corresponding to the increased expression of miR-*fmr1*. Both miR-*fmr1* ramRNAs contained the same seed sequence complementary to the zebrafish *fmr1* gene. Notably, the miR-*fmr1-42* further contained three unique structures in its pre-miRNA sequence (Fig. **5B**), including (a) multiple loops and matched CGG sites in the stem of a relatively long hairpin precursor, (b) a nuclear import signal (NIS) motif, and (c) multiple CCG-rich DNA binding motifs. Structurally, the NIS motif may allow the entry of mature miR-*fmr1-42* into the cell nucleus and the multiple CCG-rich DNA binding motifs are likely involved in transcriptional *fmr1* silencing. In addition, the NIS motif was flanked with a short poly-A tail, which may facilitate the decay of miR-*fmr1-42* and consequently prevents the accumulation of ramRNA toxicity in the wild-type zebrafish.

Involvement of Dicer1, Rad54-like and MeCP2 Functions in ramRNA-Mediated fmr1 Gene Silencing

Using morpholino antisense oligonucleotides directed against some RNAi- and CpG methylation-associated effector genes (Fig. **4**), we found that the mechanism of miR-*fmr1*-mediated gene silencing required activities of Dicer 1 (Dcr1), Rad54-like protein (Rad54l) and methyl-CpG binding protein 2 (MeCP2), but not Drosha RNaseIII (Drsh). Given that intronic miRNA precursors can bypass the

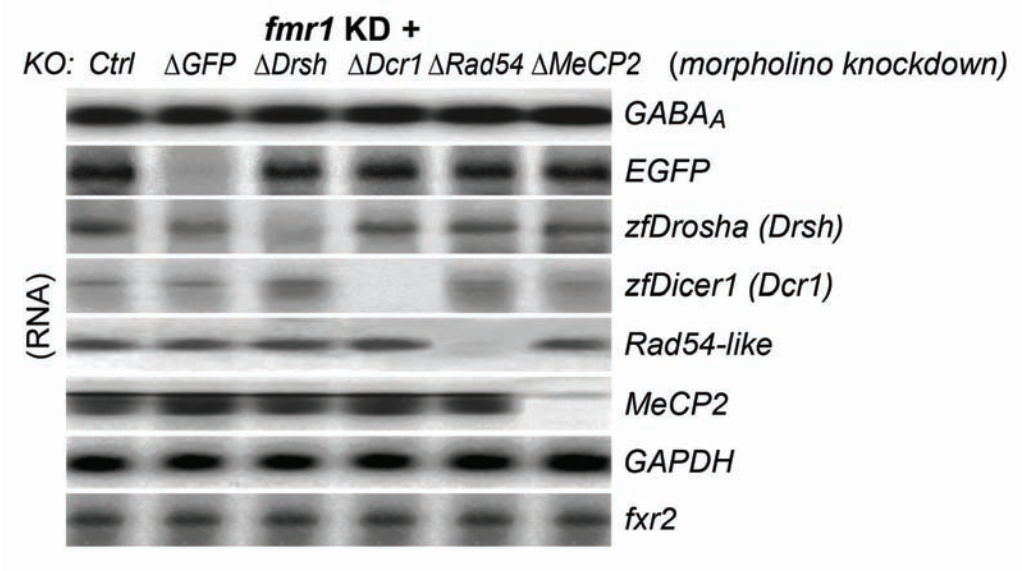

Fig. (4). Morpholino antisense oligonucleotide-mediated gene knockdown in the *fmr1* KD zebrafish. The morpholino probes were designed to target against green fluorescent protein (Δ*GFP*), zebrafish *Drosha* (Δ*Drsh*), *Dicer1* (Δ*Dcr1*), *Rad54-like* (Δ*Rad54*), and *MeCP2* (Δ*MeCP2*) (n = 5, $p < 0.01$).

Drosha processing [21], the miR-*fmr1* biogenesis may function through the same mechanism. Fig. (**3E**) showed that both miR-*fmr1* biogenesis and *fmr1* inactivation were hindered by the knockdown of miRNA-associated *Dicer1*, while only the *fmr1* inactivation rather than miR-*fmr1* biogenesis was affected when either *Rad54l* or *MeCP2* was knocked down. Fig. (**3F**) further demonstrated that the re-activation of *fmr1* gene transcription in the *fmr1* KD zebrafish was increased corresponding to the decrease of either *Rad54l* or *MeCP2* expression, confirming that both Rad54l and MeCP2 activities were required for the ramRNA-mediated *fmr1* inactivation. Previous studies have manifested that both Rad54l and MeCP2 were involved in the CpG methylation of repetitive chromatin sequences in autism spectrum disorders [22]. Likely, the same mechanism may be reiterated to cause the hyper-methylation of the *fmr1* r(CGG) expansion in FXS.

Correlation Between r(CGG)-Derived ramRNA Expression and Methylation of fmr1 Promoter in Zebrafish Neurons

The expression patterns of both miR-*fmr1* isoforms have been identified in the zebrafish brain, particularly in the lateral pallium-neocortical and cerebellar neurons, using fluorescent *in situ* hybridization (FISH) with a locked nucleic acid (LNA) probe directed against the miR-*fmr1-27* sequence (Fig. **5D**). As detected by the FISH assay in fish pallium (an equivalent of human hippocampal stratum radiatum; Fig. (**5A**) and (**5D**-sections 1 and 2), wild-type neurons contained moderate miR-*fmr1* expression only in the cytoplasm surrounding the nucleus, whereas the *fmr1* KD neurons presented a distinct phenotype of strong miR-*fmr1* accumulation all over the dendrite, soma and nucleus. Northern blotting of the two miR-*fmr1* isoforms isolated from either the cytoplasm or nucleus of the pallium neurons further authenticated that miR-*fmr1-42* was the only ramRNA accumulated in the nucleus of the *fmr1* KD neurons (Fig. **5C**). Deletion of the NIS motif from the miR-*fmr1-42* precursor significantly increased miR-*fmr1* accumulation in the cytoplasm, but not the nucleus of the neurons, suggesting that NIS is responsible for the nuclear entry of miR-*fmr1-42*. Corresponding to the nuclear miR-*fmr1-42* accumulation, a significant increase of epigenetic DNA methylation in the *fmr1* 5'-promoter upstream region was also identified by bisulfite PCR and sequencing assays (Fig. **1**). The elevation of DNA methylation was mostly observed in the CpG-rich binding sites of some *fmr1*-associated transcriptional cofactors, such as NRF1 (GCGCGC), SP1 (GC box) and USF1/USF2 (E box). It has been previously reported that preventing the accessibility of these transcriptional cofactors leads to transcriptional *fmr1* inactivation and FXS [23].

RamRNA-Induced Phenotypic Changes of fmr1 KD Neurons

Changes of neurite growth and synaptic connectivity have been observed in the *fmr1* KD fish brain, reminiscent of human FXS (Fig. **6**). In fish lateral pallium, wild-type neurons presented normal neurite growth and branching dendrification, whereas *fmr1* KD neurons exhibited long stripe dendrites similar to those found in the FXS hippocampal-neocortical junction [24, 25]. High density of long, immature dendritic spines was also observed, indicating failure in forming normal synaptic connections between these *fmr1* KD neurons (Fig. **6**, most right panel). In FXS patients, changes in spine shape were linked to the absence of FMRP function [26]. FMRP is a translational inhibitor associated with local protein synthesis of certain mRNA species involved in neurite growth and synaptic connection, leading to a crucial step for eliminating immature synapses and enhancing synaptic strength during brain development [27-29]. Therefore, the miR-*fmr1*-mediated fmrp suppression may prevent synaptic strengthening and block the local protein-synthesis-dependent synaptic connections, resulting in a cascade of events that FXS is strongly implicated. These findings may provide a new insight into the mechanism by which the shape alteration takes place in FXS dendritic spines.

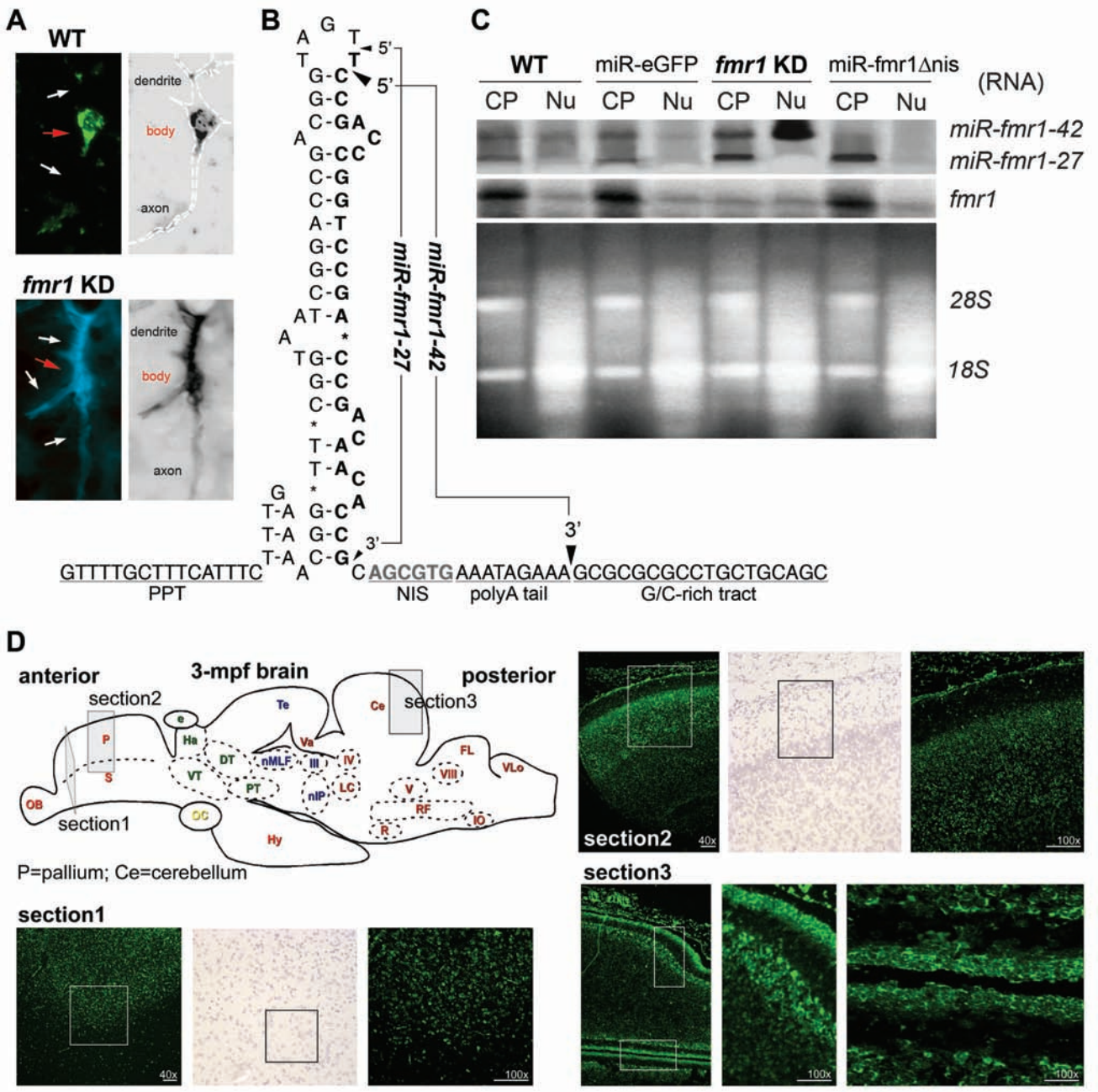

Fig. (5). Correlation between intracellular miR-*fmr1* distribution and *fmr1* promoter methylation. (**A**) Different miR-*fmr1* expression patterns between wild-types (WT) and the *fmr1* KD zebrafish, shown by fluorescent *in situ* hybridization (FISH). (**B**) Sequence and structure of the identified miR-*fmr1* precursor. From the 5' to 3' end, motifs included a poly-pyrimidine tract (PPT), a pre-miR-*fmr1-27* hairpin structure, a nuclear import signal (NIS), a short poly(A) tail, and a G/C-rich tract. (**C**) Northern blots showing distribution patterns of the two miR-*fmr1* isoforms and *fmr1* mRNA in the cytoplasmic (CP) and nuclear (Nu) compartments of the fish pallium neurons (n = 4, $p < 0.01$). Samples isolated from four different zebrafish strains were labeled from left to right: the wild-types (WT), transgenics with a scrambled miRNA against eGFP (miR-*eGFP*), the *fmr1* KD, and transgenics transfected with only the miR-*fmr1-27* (miR-*fmr1*Δnis). (**D**) Tissue expression patterns of miR-*fmr1* in the wild-type three-month-old zebrafish brain, showing the results of *in situ* hybridization in the cross section of lateral pallium (section 1), the longitudinal section of pallium-neocortical junction (section 2), and the longitudinal section of cerebellum (section 3).

RamRNA-Induced Fragile X-Like Syndrome in Zebrafish Brain Circuits

Impairment of synaptic plasticity is a major symptom of human FXS. Two types of synaptic plasticity are dependent on protein synthesis: long-term potentiation (LTP) and long-term depression (LTD). LTP is a long-term increase in synaptic strength in response to high-frequency stimulation, whereas LTD is a decrease in the strength of the same synapses after prolonged, low frequency stimulation. Both LTP and LTD underline the encoding activities of new declarative

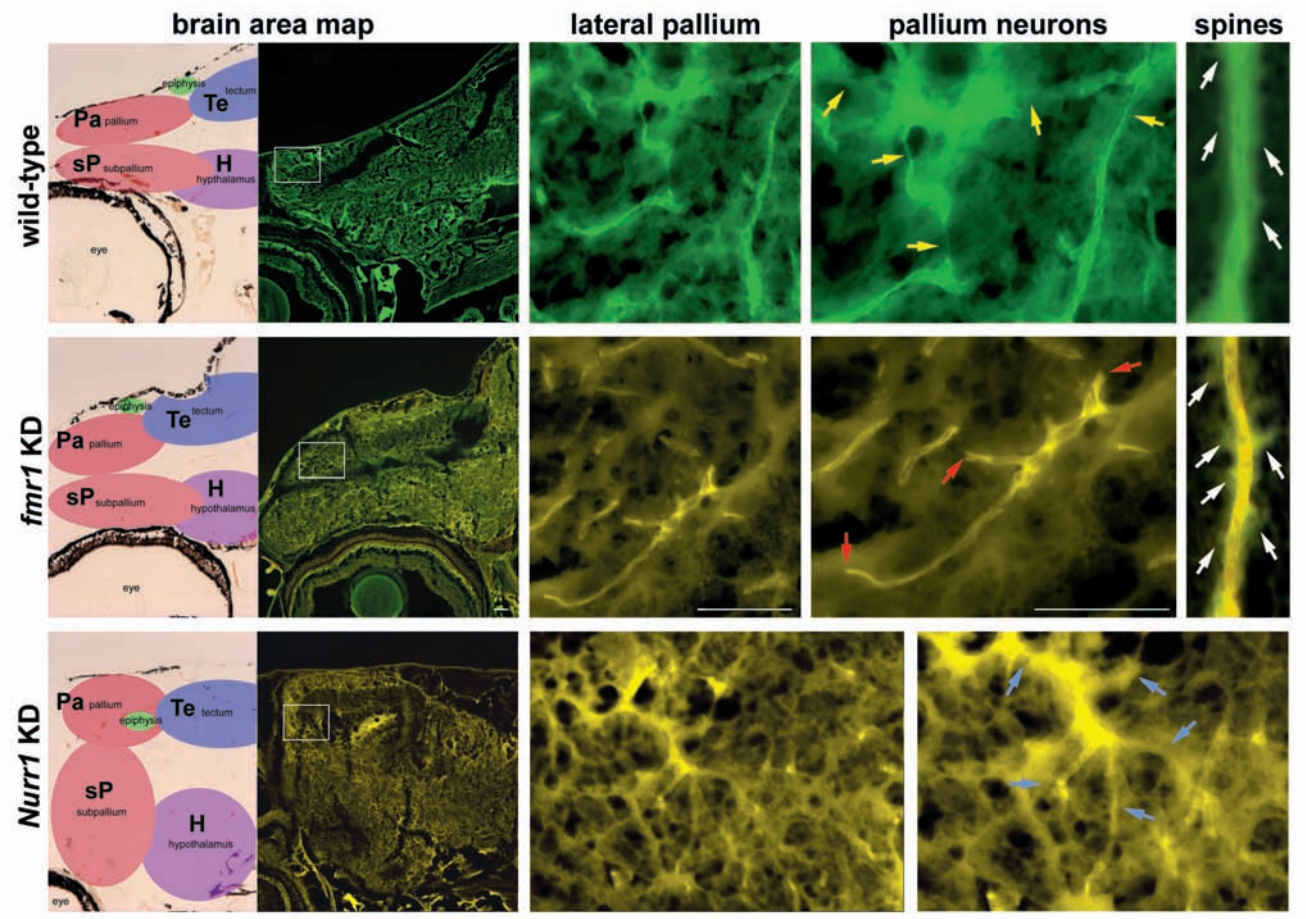

Fig. (6). Morphological changes of lateral pallium neurons in the transgenic zebrafish with *fmr1*-knockdown (*fmr1* KD) (middle row) and *Nurr1*-knockdown (*Nurr1* KD) (bottom row) as compared to the wild-types (top row). The wild-type Tg(*actin*-GAL4:UAS-gfp) zebrafish displayed an *actin* promoter-driven green eGFP protein, while the transgenics co-expressed a red rGFP reporter protein and thus converted the affected neuron color to yellow, as shown by the fluorescent 3D-micrograph. Different neuronal connectivity was observed, including normal (yellow arrows), disrupted (red arrows), tangled (gray arrows) neurite growth and synaptic circuits. White arrows indicated the formation of dendritic spines. The *Nurr1* KD transgenics were generated by retroviral transfection of miR-739, which targeted against *Nurr1* but not *fmr1*. Abbreviations indicated: Pa, pallium; sP, subpallium; Te, tectum; H, hypothalamus.

memories [30]. LTP in hippocampus is a learning-associated form of synaptic plasticity that is highly involved in the shape change of dendritic spines. Theta activity (3-8 Hz) is the major late-phase (protein-synthesis-dependent) stimulation during the hippocampal encoding of long-term memory [30]. In three-month-old male *fmr1* KD zebrafish, theta burst-stimulated synapses of the pallium-neocortical junction (an equivalent of human hippocampal CA1-CA3) were observed to exhibit diminished LTP compared to the wild-type controls (Fig. **7A**). The decreased LTP remained even after the blockade of metabotropic GABA receptor ($GABA_A$)-dependent synaptic inhibition by picotoxin treatment, similar to the human FXS neuron response in the hippocampal CA3 region (Fig. **7B**). Furthermore, a corresponding decrease of the input-output currents, measured at the peak amplitude of dendritic field excitatory postsynaptic potentials (fEPSPs), was consistent with the diminished LTP (Fig. **7E**), which indicated a lower excitatory membrane response in the *fmr1* KD neurons. Given that the excitability of LTP of GABAergic neurons is mediated by activation of group 1 metabotropic glutamate receptor (mGluR1) [31], understanding the interaction between FMR1 and mGluR1 may shed light on the mechanism underlying LTP diminishment in FXS.

Post-synaptic stimulation of mGluR has been reported to increase FMRP synthesis and subsequently triggers internalization of α-amino-3-hydroxy-5-methyl-4-isoxazole propionic acid (AMPA) receptors, a quenching process important for rapid reverse of synaptic LTD changes [32, 33]. The loss of FMRP in hippocampal neurons may over-amplify this LTD response and thus decreases the excitability of LTP, as shown in Fig. (**7C**-**D**). This augmented LTD was triggered by treatment of mGluR-specific agonist, 3,5-dihydroxyphenyglycine (DHPG) in the presence of a *N*-methyl-D-aspartate receptor (NMDAR) antagonist D-2-amino-5-phosphonovalerate (D-APV) to prevent NMDAR-mediated LTD. Co-treatment of DHPG with another mGluR antagonist, LY341495, inhibited all LTD, which confirmed that such LTD augmentation was mGluR-dependent (mGluR-LTD). Further treatment of anisomycin, a protein synthesis inhibitor, with DHPG reduced the mGluR-LTD elevation in the wild-type neurons (Fig. **7C**), except for the *fmr1* KD neurons (Fig. **7D**). These findings suggested that

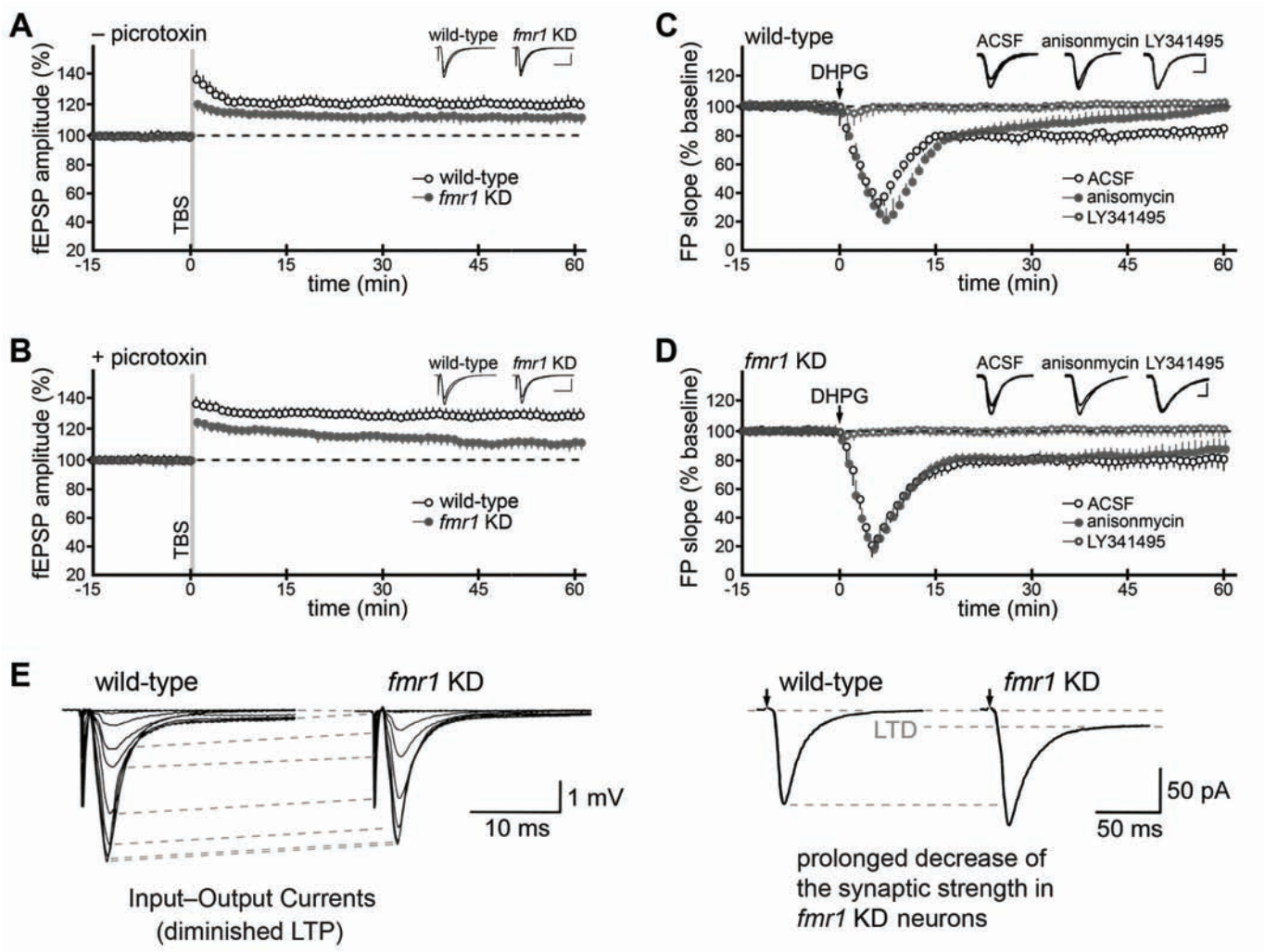

Fig. (7). Alterations of LTP and LTD in the *fmr1* KD fish pallium (hippocampus). (**A**) A significant decrease of theta burst stimulation (TBS)-induced LTP detected in the *fmr1* KD neurons (solid dot) compared to the wild-types (open circle) around the pallium-neocortical junction. The amplitude (%) of field excitatory postsynaptic potentials (fEPSPs) was measured up to sixty minutes after TBS. (**B**) The decreased LTP of (A), sustained after metabotropic $GABA_A$-dependent synaptic inhibition blocked by 20 μM picotoxin treatment. (**C**) Normal LTD stimulated by an mGluR-agonist DHPG (100 μM in ACSF for 2 min, open circle) in wild-type pallium neurons. Pre-treatment of a protein synthesis inhibitor, anisomycin (20 μM, solid dot), reduced the DHPG-induced LTD response. However, the co-treatment of a broad mGluR-antagonist, LY341495 (100 μM in ACSF for 2 min, gray circle), completely inhibited the DHPG-induced LTD. Synaptic induction of mGluR-LTD was defined by the initial slope of the field potentials (FP), shown by the percentage of each treatment baseline averaged. (**D**) Elevated LTD found in the *fmr1* KD fish pallium. All treatments were the same as (C); nevertheless, the anisomycin treatment failed to affect the DHPG-induced LTD. Changes of both LTP and LTD reflected certain abnormal synaptic circuits in the hippocampal neurons, which hindered the learning and cognitive function of the brain. (**E**) Standard curves of synaptic responses in pallium slices from three-month-old male wild-type and *fmr1* KD zebrafish. Synaptic input-output fEPSP curves were evoked by varying bipolar current intensities, from 5.0, 10.0, 15.0, 25.0, 45.0, 65.0, 100.0 to 155.0 μA (pulse duration 0.1 ms). Calibration: 1 mV, 10 ms. Pulse-induced depression curves were measured at 40 μA for 125 ms. Calibration: 50 pA, 50 ms.

the mGluR-LTD elevation in *fmr1* KD neurons could occur in the absence of new protein synthesis. Seeing that FMRP functions to suppress the translation of certain mRNAs involved in normal neural development and plasticity [5, 6], its deficiency caused by the ramRNA-mediated *FMR1* inactivation may lead to excessive accumulation of the FMRP-suppressed proteins in the FXS neurons, and ultimately leading to the protein-synthesis-independent mGluR-LTD elevation and LTP diminishment.

DISCUSSION

Overall, the present study identified a novel etiological mechanism of FXS (Fig. **8**), in which excessive expression of ramRNAs derived from the *FMR1* 5'-UTR r(CGG) expansion could cause nuclear ramRNA accumulation and hence inactivated the *FMR1* gene transcription through promoter DNA methylation. Dicer1 rather than Drosha was required for the ramRNA biogenesis, while Rad54l and

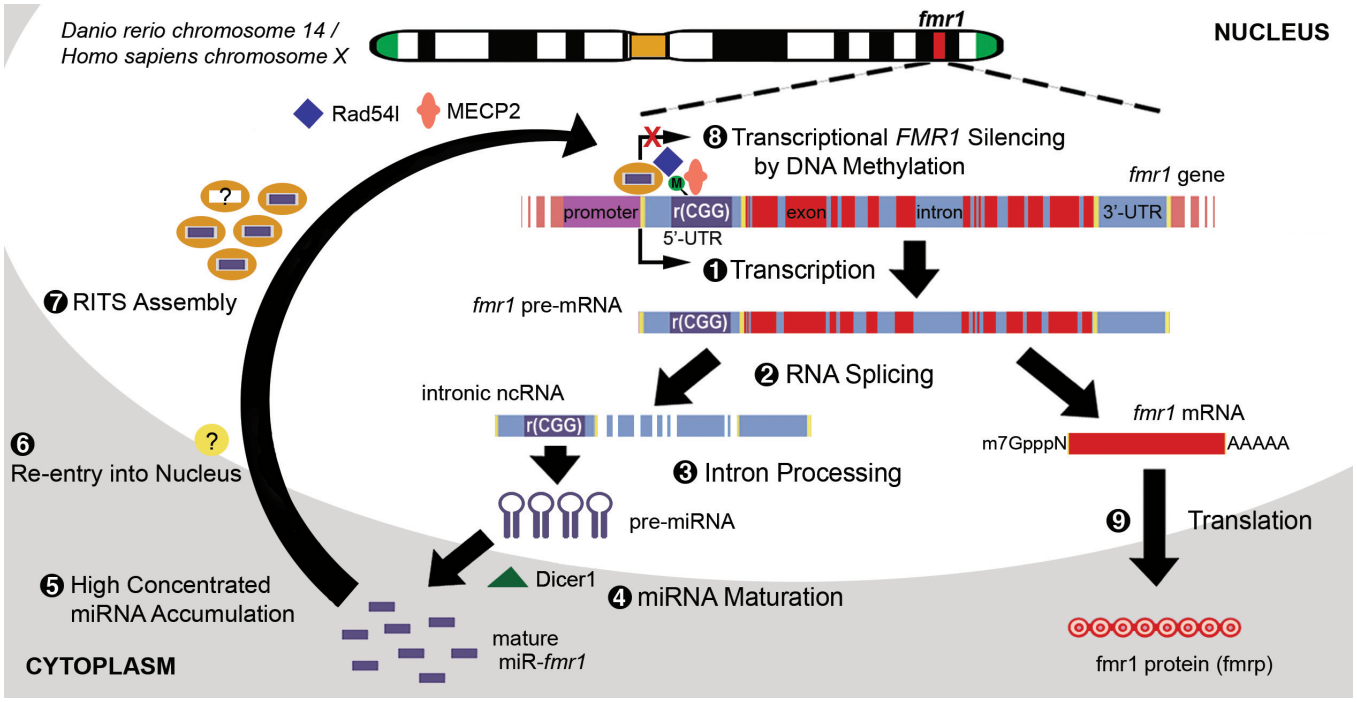

Fig. (8). Proposed mechanism of the ramRNA-mediated *FMR1* inactivation in FXS-like mental retardation. Expansion of trinucleotide CGG repeats [r(CGG)] in the fragile X mental retardation 1 (*FMR1*) gene that encodes FMRP underlies FXS-related disorders. Repeats expanded over 200 copies (full mutation) led to loss of FMRP expression. Based on the present study, the pathological progression of such FMRP deficiency includes nine steps: first, transcription of the *FMR1* gene starts at a very early embryonic stage (i.e. day 10 human embryo and 12 hour post-fertilization zebrafish). Second, RNA splicing and processing remove the 5'-UTR r(CGG) expansion from the mature *FMR1* mRNA. Third, the 5'-UTR r(CGG) expansion is further processed into repeat-associated miRNA (ramRNA) precursors by a certain RNaseIII. Fourth, the ramRNA precursors are exported to cytoplasm and cleaved into mature miR-*FMR1*s by Dicer1. Fifth, high concentrated miR-*FMR1*s accumulate in cytoplasm around the cell nucleus. Sixth, some miR-*FMR1*s tailed with a nuclear import signal (NIS) can re-enter the cell nucleus. Seventh, the nuclear miR-*FMR1*s gradually accumulate and form RNA-induced transcriptional silencing (RITS) assembly near the *FMR1* promoter. Eighth, the RITS assembly interacts with Rad541 and MeCP2 to cause transcriptional *FMR1* gene inactivation through a CpG DNA methylation mechanism. Last, the ramRNA-mediated *FMR1* inactivation results in the deficiency of FMRP, the most prevalent event observed in over 99% of the FXS patients.

MeCP2 played a crucial role in the RITS assembly of the ramRNAs responsible for the *FMR1* promoter methylation. The pathological outcomes of this ramRNA-mediated *FMR1* gene silencing was corresponded to the neurodegenerative and cognitive impairments in FXS disorders, like neuronal deformity, immature synapse formation, long dendritic spine shaping, LTP diminishment, and mGluR-LTD augment. In this study, we over-expressed one third of the wild-type *fmr1* 5'-UTR r(CGG) expansion and found one nuclear ramRNA, miR-*fmr1-42*; it is estimated that the full *FMR1* r(CGG) expansion in FXS may generate over 12 nuclear ramRNAs. These findings signify a similarity between the ramRNA-mediated *fmr1* KD animal model and human FXS, which may shed light on new therapeutic intervention. Furthermore, this animal model may provide insights into the mechanism of microsatellite-like nucleotide repeats in brain development for understanding its effect on human intelligence quotient (IQ). Given that there are many different microsatellite-like nucleotide repeats in the human genome, which may encode a variety of ramRNAs, this model may be used for exploiting the functional roles of these ramRNAs *in vivo* as a forthcoming challenge.

ACKNOWLEDGEMENTS

This study was supported by NIH/NCI Grant CA-85722, USA.

REFERENCES

[1] Handa V, Saha T, Usdin K. The fragile X syndrome repeats form RNA hairpins that do not activate the interferon-inducible protein kinase, PKR, but are cut by Dicer. Nucleic Acids Res 2003; 31: 6243-8.

[2] Krol J, Fiszer A, Mykowska A, Sobczak K, de Mezer M, Krzyzosiak WJ. Ribonuclease dicer cleaves triplet repeat hairpins into shorter repeats that silence specific targets. Mol Cell 2007; 25: 575-86.

[3] Jin P, Alisch RS, Warren ST. RNA and microRNAs in fragile X mental retardation. Nat Cell Biol 2004; 6: 1048-53.

[4] Hagerman RJ, Staley LW, O'Conner R, *et al*. Learning-disabled males with a fragile X CGG expansion in the upper premutation size range. Pediatrics 1996; 97: 122-6.

[5] Eberhart DE, Malter HE, Feng Y, Warren ST. The fragile X mental retardation protein is a ribonucleoprotein containing both nuclear localization and nuclear export signals. Hum Mol Genet 1996; 5: 1083-91.

[6] Tamanini F, Van Unen L, Bakker C, *et al*. Oligomerization properties of fragile-X mental-retardation protein (FMRP) and the fragile-X-related proteins FXR1P and FXR2P. Biochem J 1999; 343 Pt 3: 517-23.

[7] Sutcliffe JS, Nelson DL, Zhang F, *et al.* DNA methylation represses FMR1 transcription in fragile X syndrome. Hum Mol Genet 1992; 1: 397-400.

[8] Lin SL, Chang SJE, Ying SY. First *in vivo* evidence of microRNA-induced fragile X mental retardation syndrome. Mol Psychiatry 2006; 11: 616-7.

[9] Tropepe V, Sive HL. Can zebrafish be used as a model to study the neurodevelopmental causes of autism? Genes Brain Behav 2003; 2: 268-81.

[10] Tucker B, Richards R, Lardelli M. Expression of three zebrafish orthologs of human FMR1-related genes and their phylogenetic relationships. Dev Genes Evol 2004; 214: 567-74.

[11] van 't Padje S, Engels B, Blonden L, *et al.* Characterization of FMRP in zebrafish: evolutionary dynamics of the fmr1 gene. Dev Genes Evol 2005; 215: 198-206.

[12] Gaiano N, Amsterdam A, Kawakami K, Allende M, Becker T, Hopkins N. Insertional mutagenesis and rapid cloning of essential genes in zebrafish. Nature 1996; 383: 829-32.

[13] Lin SL, Ying SY. Transgene-like animal models using intronic microRNAs. Methods Mol Biol 2006; 342: 321-43.

[14] Xia XG, Zhou H, Samper E, Melov S, Xu Z. Pol II-expressed shRNA knocks down Sod2 gene expression and causes phenotypes of the gene knockout in mice. PLoS Genet 2006; 2: e10.

[15] Lopez-Bendito G, Shigemoto R, Kulik A, Vida I, Fairen A, Lujan R. Distribution of metabotropic GABA receptor subunits GABAB1 a/b and GABAB2 in the rat hippocampus during prenatal and postnatal development. Hippocampus 2004; 14: 836-48.

[16] Selby L, Zhang C, Sun QQ. Major defects in neocortical GABAergic inhibitory circuits in mice lacking the fragile X mental retardation protein. Neurosci Lett 2007; 412: 227-32.

[17] Lin SL, Chang D, Wu DY, Ying SY. A novel RNA splicing-mediated gene silencing mechanism potential for genome evolution. Biochem Biophys Res Commun 2003; 310: 754-60.

[18] Lin SL, Ying SY. Gene silencing *in vitro* and *in vivo* using intronic microRNAs. Methods Mol Biol 2006; 342: 295-312.

[19] Sprague J, Clements D, Conlin T, *et al*. The Zebrafish Book, M. Westerfield, Ed. The Zebrafish Information Network (ZFIN): the zebrafish model organism database. Nucleic Acids Res 2003; 31: 241.

[20] Kimmel CB, Ballard WW, Kimmel SR, Ullmann B, Schilling TF. Stages of embryonic development of the zebrafish. Dev Dyn 1995; 203: 253.

[21] Ruby JG, Jan CH, Bartel DP. Intronic microRNA precursors that bypass Drosha processing. Nature 2007; 448: 83-6.

[22] Lopez-Rangel E, Lewis ME. Loud and clear evidence for gene silencing by epigenetic mechanisms in autism spectrum and related neurodevelopmental disorders. Clin Genet 2006; 69: 21-2.

[23] Kumari D, Gabrielian A, Wheeler D, Usdin K. The roles of Sp1, Sp3, USF1/USF2 and NRF-1 in the regulation and three-dimensional structure of the Fragile X mental retardation gene promoter. Biochem J 2005; 386: 297-303.

[24] Huber KM, Gallagher SM, Warren ST, Bear MF. Altered synaptic plasticity in a mouse model of fragile X mental retardation. Proc Natl Acad Sci USA 2002; 99: 7746-50.

[25] Irwin SA, Christmon CA, Grossman AW, *et al.* Greenough, Fragile X mental retardation protein levels increase following complex environment exposure in rat brain regions undergoing active synaptogenesis. Neurobiol Learn Mem 2005; 83: 180-7.

[26] Irwin SA, Patel B, Idupulapati M, *et al*. Greenough, Abnormal dendritic spine characteristics in the temporal ans visual cortices of patients with fragile-X syndrome: a quantitative examination. Am J Med Genet 2001; 98: 161-7.

[27] Brown V, Jin P, Ceman S, *et al.* Microarray identification of FMRP-associated brain mRNAs and altered mRNA translational profiles in fragile X syndrome. Cell 2001; 107: 477-87.

[28] Li Z, Zhang Y, Ku L, Wilkinson KD, Warren ST, Feng Y. The fragile X mental retardation protein inhibits translation *via* interacting with mRNA. Nucleic Acids Res 2001; 29: 2276-83.

[29] Jin P, Zarnescu DC, Zhang F, *et al*. RNA-mediated neurodegeneration caused by the fragile X premutation rCGG repeats in *Drosophila*. Neuron 2003; 39: 739-47.

[30] Axmacher N, Mormann F, Fernandez G, Flger CE, Fell J. Memory formation by neuronal synchronization. Brain Res Rev 2006; 52: 170-82.

[31] Patenaude C, Chapman CA, Bertrand S, Congar P, Lacaille JC. GABAB receptor- and metabotropic glutamate receptor-dependent cooperative long-term potentiation of rat hippocampal GABAA synaptic transmission. J Physiol 2003; 553: 155-67.

[32] Snyder EM, Philpot BD, Huber KM, Dong X, Fallon JR, Bear MF. Internalization of ionotropic glutamate receptors in response to mGluR activation. Nat Neurosci 2001; 4: 1079-85.

[33] Nosyreva ED, Huber KM. Metabotropic receptor-dependent long-term depression persists in the absence of protein synthesis in the mouse model of fragile X syndrome. J Neurophysiol 2006; 95: 3291-5.

Received: October 29, 2008 Revised: November 12, 2008 Accepted: November 12, 2008